

A three field weak formulation for integration of the equations of motion of multibody systems subject to equality constraints

Elias Paraskevopoulos*, Nikolaos Potosakis* and Sotirios Natsiavas*

**Department of Mechanical Engineering, Aristotle University, Thessaloniki, Greece*

Summary. This study focuses on dynamics of a class of discrete mechanical systems subject to equality motion constraints. Following a proper application of Newton's law of motion on configuration manifolds possessing general geometric properties (i.e., metric and connection), a new set of equations of motion is first obtained as a system of second order ordinary differential equations (ODEs). Then, a suitable weak formulation is developed and applied, providing a reliable foundation for performing an efficient numerical integration based on an augmented Lagrangian scheme. Finally, a set of numerical results is presented for selected mechanical examples, illustrating the advantages of the new approach.

Introduction - Motivation

Research on the dynamics of mechanical systems subject to motion constraints is a traditional and favorable topic among researchers with different backgrounds (e.g., [1-4]). This is in part due to the fact that this area of Analytical Mechanics is still challenging and several theoretical aspects related to it remain unexplored and are amenable to improvement, despite the long tradition on the subject. Another driving factor is that a better understanding of the fundamentals in this area provides a stronger foundation and offers substantial help in the efforts to solve difficult engineering problems by deriving and employing new, more advanced, accurate and robust numerical techniques [5,6]. This in turn leads to useful design gains in many areas, including mechanisms, robotics, machinery, biomechanics, automotive and aerospace structures.

Typically, the equations of motion for this class of systems are derived and cast in the form of a set of differential-algebraic equations (DAEs) of high index. However, both the theoretical and the numerical treatment of DAEs is a delicate and difficult task [7]. For this reason, many attempts have been performed in the past in an effort to cure the problems related to a DAE modeling. Over the years, it has become apparent that many of the theoretical questions in the area of Analytical Dynamics, related to engineering problems, can be answered in an illustrative and complete way by employing fundamental concepts of differential geometry [8,9]. Based on this observation, the main objective of this work is to use such concepts in order to provide a better theoretical foundation and to develop an appropriate numerical scheme for treating a class of constrained mechanical systems.

The new approach assigns appropriate inertia, damping and stiffness properties to the constraints. As a result, the equations of motion are second order ODEs in both the generalized coordinates and the Lagrange multipliers, arising from the constraint action [10,11]. This, in turn, leads to elimination of the singularities associated with DAE or penalty formulations. As a consequence, there is no need to introduce artificial parameters for scaling and stabilization. In addition, the geometrical properties of the original manifold are kept unchanged by the additional constraints. This preserves the properties of the special curves of the manifold employed in the numerical discretization and leads to major advantages compared to previous work in the field of computational Multibody Dynamics [5,6]. These equations are first put in a convenient weak form. Moreover, the position, velocity and momentum type quantities are assumed to be independent, forming a three field set of equations [12,13]. In particular, the weak velocities and the strong time derivatives of all the coordinates involved in the formulation are related through a new set of Lagrange multipliers, which are shown to represent momentum type variables. Next, the weak formulation developed is employed as a basis for producing suitable time integration schemes for the class of systems examined. One such scheme was developed for the purposes of this study. The validity and efficiency of this scheme was tested and illustrated by applying it to a number of characteristic example mechanical systems. Among other things, the results obtained verify that the scheme developed passes successfully all the tests related to a special set of challenging benchmark problems, chosen by the multibody dynamics community [14]. In addition, the same scheme was also applied successfully to a number of large scale industrial applications as well.

The organization of this paper is as follows. First, the strong form of the equations of motion governing the dynamics of an unconstrained discrete mechanical system is presented briefly in the following section. Then, the corresponding weak form of these equations is derived in the third section. Next, the weak form of the equations of motion for the class of constrained multibody systems examined is derived and presented in the fourth section. Based on this form, a temporal discretization scheme was developed and numerical results were obtained for several mechanical examples. Some characteristic numerical results are presented in the fifth section.

Application of Newton's law of motion on a manifold

This work examines a class of mechanical systems whose position is determined by a finite number of generalized coordinates $q = (q^1, \dots, q^n)$, at any time instance t [1,9]. The motion of such a system can be represented by the motion of a fictitious point, say p , along a curve $\gamma = \gamma(t)$ in an n -dimensional manifold M , the configuration space of the

system. Moreover, the tangent vector $\underline{v} = d\gamma/dt$ to this curve belongs to an n -dimensional vector space, the tangent space of the manifold at p , denoted by $T_p M$ [4]. By construction, for any point p of M , a coordinate map φ can be defined by

$$q = \varphi(p) \quad (1)$$

acting from a neighborhood of p on M to the Euclidean space \mathbb{R}^n . Then, by adopting the usual summation convention on repeated indices, each tangent vector at point p can be expressed in the form

$$\underline{v}(t) = v^i(t) \underline{e}_i, \quad (2)$$

where $\mathfrak{B}_e = \{\underline{e}_1 \dots \underline{e}_n\}$ is a coordinate basis for space $T_p M$. Likewise, one can define the dual space to $T_p M$, denoted by $T_p^* M$, with elements known as covectors. In dynamics, a correspondence between a covector \underline{u}^* and a vector \underline{u} is established through the dual product

$$\underline{u}^*(\underline{w}) \equiv \langle \underline{u}, \underline{w} \rangle, \quad \forall \underline{w} \in T_p M, \quad (3)$$

where $\langle \cdot, \cdot \rangle$ denotes the inner product of vector space $T_p M$ [8]. In this way, to each basis $\{\underline{e}_i\}$ (with $i=1, \dots, n$) of $T_p M$, a dual basis $\{\underline{e}^i\}$ can be established for $T_p^* M$ by employing the condition $\underline{e}^i(\underline{e}_j) = \delta_j^i$. Then, determination of the true path of motion (or the natural trajectory) on a manifold is based on application of Newton's second law in the form

$$\nabla_{\underline{v}} \underline{p}_M^* = \underline{f}_M^*, \quad (4)$$

where \underline{v} is the tangent vector of the natural trajectory $\gamma(t)$, while $\underline{f}_M^* = f_i \underline{e}^i$ represents the applied force [1,9]. Moreover, the generalized momentum is defined as the covector corresponding to the velocity vector, i.e., $\underline{p}_M^* \equiv \underline{v}^*$.

Then, if $\underline{v} = v^i \underline{e}_i$ and $\underline{p}_M^* = p_i \underline{e}^i$, application of Eq. (3) leads to

$$p_i = g_{ij} v^j, \quad (5)$$

where the quantities $g_{ij} = \langle \underline{e}_i, \underline{e}_j \rangle$ represent the components of the metric tensor at point p . These quantities are selected to coincide with the elements of the mass matrix of the system, defined through the kinetic energy. Finally, the covariant differential of the covector field $\underline{p}_M^*(t)$ on M along a vector \underline{v} of $T_p M$ is evaluated by

$$\nabla_{\underline{v}} \underline{p}_M^*(t) = (\dot{p}_k - \Lambda_{ik}^j v^i p_j) \underline{e}^k. \quad (6)$$

where ∇ is the affine connection of the manifold. The components Λ_{ij}^k of the connection ∇ in the basis of $T_p M$ are known as affinities [2,9].

Weak form of Newton's law on a manifold with no motion constraints

Through the definition of a class of special covectors (called Newton covectors, see [11]) by

$$\underline{h}_M^* \equiv \nabla_{\underline{v}} \underline{p}_M^* - \underline{f}_M^*, \quad (7)$$

the equations of motion (4) at any point on a configuration manifold M can be put in the form

$$\underline{h}_M^* = \underline{0}. \quad (8)$$

Therefore, when there exist no motion constraints, it should be true that

$$\underline{h}_M^*(\underline{w}) = 0 \Rightarrow \int_{t_1}^{t_2} \underline{h}_M^*(\underline{w}) dt = 0, \quad \forall \underline{w} \in T_p M \quad (9)$$

along a natural trajectory on the manifold and within any time interval $[t_1, t_2]$. Manipulation of the last integral requires application of integration by parts of the covariant derivative appearing in Eq. (7). This is achieved by employing the identity

$$\nabla_{\underline{v}} (\underline{p}_M^*(\underline{w})) = (\nabla_{\underline{v}} \underline{p}_M^*)(\underline{w}) + \underline{p}_M^*(\nabla_{\underline{v}} \underline{w}), \quad (10)$$

which can be interpreted as a Leibniz rule on differentiation. Then, the following expression is obtained

$$\int_{t_1}^{t_2} [\nabla_{\underline{v}} (\underline{p}_M^*(\underline{w})) - \underline{p}_M^*(\nabla_{\underline{v}} \underline{w}) - \underline{f}_M^*(\underline{w})] dt = 0. \quad (11)$$

Finally, after an integration by parts of the first term inside the integral, the last equation becomes

$$[p_M^*(\underline{w})]_{t_1}^{t_2} - \int_{t_1}^{t_2} [p_M^*(\nabla_{\underline{v}} \underline{w}) + f_M^*(\underline{w})] dt = 0. \quad (12)$$

This equation represents the so called weak form of the equations of motion [15]. In essence, it constitutes an alternative way to determine the true history of the coordinates (i.e., position) and velocities of a mechanical system satisfying the law of motion, as expressed by Eq. (4) originally.

Further manipulation of the weak form of the equations of motion (12) involves differentiations along the vectors \underline{v} and \underline{w} . This requires the construction of two smooth vector fields on M . The first of these can be constructed by considering the tangent vector \underline{v} at each point of the natural trajectory $\gamma(t)$. The second vector field can then be created by introducing another vector \underline{w} of the tangent space at each point of the same trajectory, which can be arbitrary. Therefore, a variation of any scalar function f is defined as the derivative of f along vector \underline{w} , by

$$\delta f \equiv \underline{w}(f) = f_{,i} w^i. \quad (13)$$

Likewise, the differential of f is defined by

$$df \equiv \underline{v}(f) = f_{,i} v^i. \quad (14)$$

Weak form of Newton's law on a manifold with bilateral constraints

Next, consider systems subject to an additional set of k scleronomic constraints, which can be put in the form

$$\dot{\psi}(q, \underline{v}) \equiv A(q) \underline{v} = \underline{0}, \quad (15)$$

where \underline{v} is a vector in $T_p M$ and $A = [a_i^R]$ is a known $k \times n$ matrix. In the special case where constraint is holonomic, these equations can be integrated and written in the algebraic form

$$\phi^R(q) = 0. \quad (16)$$

Based on the above, the equations of motion of the class of systems examined can be cast in the form

$$\underline{h}_M^* = \underline{h}_C^* \quad (17)$$

on the original manifold M [11], with

$$\underline{h}_M^* = h_i \underline{e}^i = [(g_{ij} v^j) \cdot - \Lambda_{ti}^m g_{mj} v^j v^t - f_i] \underline{e}^i \quad \text{and} \quad \underline{h}_C^* = \sum_{R=1}^k [(\bar{m}_{RR} \dot{\lambda}^R) \cdot + \bar{c}_{RR} \dot{\lambda}^R + \bar{k}_{RR} \lambda^R - \bar{f}_R] a_i^R \underline{e}^i. \quad (18)$$

In the last relation, the convention on repeated indices does not apply to index R . Moreover, the coefficients

$$\bar{m}_{RR} = c_R^i g_{ij} c_R^j, \quad \bar{c}_{RR} = -c_R^i \frac{\partial f_i}{\partial v^j}(q, \underline{v}, t) c_R^j, \quad \bar{k}_{RR} = -c_R^i f_{i,j}(q, \underline{v}, t) c_R^j, \quad \bar{f}_R = c_R^i f_i(q, \underline{v}, t) \quad (19)$$

represent an equivalent mass, damping, stiffness and forcing quantity, respectively, obtained through a projection along a special direction \underline{c}_R on $T_p M$ [11]. Specifically, the components of the n -vector \underline{c}_R are selected to satisfy

$$a_i^R c_R^i = 1. \quad (20)$$

If generalized (true) coordinates are used, which means that $v^i = \dot{q}^i$, Eq. (17) represents a set of n second order coupled ODEs in the $n+k$ unknowns q^i and λ^R . The additional information needed for a complete mathematical formulation is obtained by incorporating the k equations of the constraints. In particular, for each holonomic and non-holonomic constraint, a second order ODE is obtained, with form

$$(\bar{m}_{RR} \dot{\phi}^R) \cdot + \bar{c}_{RR} \dot{\phi}^R + \bar{k}_{RR} \phi^R = 0 \quad \text{and} \quad (\bar{m}_{RR} \dot{\psi}^R) \cdot + \bar{c}_{RR} \dot{\psi}^R = 0, \quad (21)$$

respectively. Taking into account the new set of equations of motion (17), Eq. (9) is first modified accordingly to

$$\int_{t_1}^{t_2} (\underline{h}_M^* - \underline{h}_C^*)(\underline{w}) dt = 0, \quad \forall \underline{w} \in T_p M. \quad (22)$$

Next, consider a holonomic constraint, as expressed by Eq. (16). It is easy to verify that the following is satisfied

$$\int_{t_1}^{t_2} [(\bar{m}_{RR} \dot{\phi}^R) \cdot + \bar{c}_{RR} \dot{\phi}^R + \bar{k}_{RR} \phi^R] \delta \lambda^R dt = 0,$$

for an arbitrary multiplier $\delta \lambda^R$. A similar expression is obtained for each non-holonomic constraint as well.

In a weak formulation, it is advantageous to consider the position, velocity and momentum variables as independent [16-18]. For this, a new velocity field \underline{v} is introduced on manifold M , which should eventually be forced to become identical to the true velocity field through the components π_i of a covector, representing a set of Lagrange multipliers.

A similar action can be taken for the velocity components $\dot{\lambda}^R$, by introducing another set of Lagrange multipliers, σ_R . Likewise, one can relate the strong time derivatives v^i and $\dot{\lambda}^R$ of the position type variables to weak velocities, v^i and μ^R , through two new sets of Lagrange multipliers, denoted by $\delta\pi_i$ and $\delta\sigma_R$, respectively. To achieve these tasks, the weak form expressed by Eq. (22) should be augmented by the terms

$$\int_{t_1}^{t_2} [\pi_i(\delta v^i - \delta v^i) + \delta\pi_i(v^i - v^i)]dt \quad \text{and} \quad \int_{t_1}^{t_2} [\sigma_R(\delta\mu^R - \delta\dot{\lambda}^R) + \delta\sigma_R(\mu^R - \dot{\lambda}^R)]dt. \quad (23)$$

Finally, by adding up all these terms and performing appropriate mathematical operations yields eventually the following three field set of equations

$$\begin{aligned} & (p_i - \sum_{R=1}^k a_i^R \bar{m}_{RR} \mu^R - \pi_i) w^i \Big|_{t_1}^{t_2} + \sum_{R=1}^k (\bar{m}_{RR} \dot{\phi}^R - \sigma_R) \delta\lambda^R \Big|_{t_1}^{t_2} + \int_{t_1}^{t_2} \delta\pi_i (v^i - v^i) dt + \sum_{R=1}^k \int_{t_1}^{t_2} \delta\sigma_R (\mu^R - \dot{\lambda}^R) dt \\ & + \int_{t_1}^{t_2} [(-p_i + \sum_{R=1}^k a_i^R \bar{m}_{RR} \mu^R + \pi_i) \delta v^i + \sum_{R=1}^k (\sigma_R - \bar{m}_{RR} \dot{\phi}^R) \delta\mu^R] dt - \int_{t_1}^{t_2} \{(-p_\ell + \sum_{R=1}^k a_\ell^R \bar{m}_{RR} \mu^R + \pi_\ell)(\tau_{ij}^\ell - \Lambda_{ij}^\ell + \sigma_{ij}^\ell) v^j \\ & + \sum_{R=1}^k [(\bar{c}_{RR} \mu^R + \bar{k}_{RR} \lambda^R - \bar{f}_R) a_i^R - \bar{m}_{RR} \mu^R \frac{Da_i^R}{Dt}] w^i + f_i - \frac{D\pi_i}{Dt} \} w^i dt + \sum_{R=1}^k \int_{t_1}^{t_2} (\dot{\sigma}_R + \bar{c}_{RR} \dot{\phi}^R + \bar{k}_{RR} \phi^R) \delta\lambda^R dt = 0, \end{aligned} \quad (24)$$

where the variations w^i , $\delta\lambda^R$, δv^i , $\delta\mu^R$, $\delta\pi_i$ and $\delta\sigma_R$ are independent for all $i = 1, \dots, n$ and $R = 1, \dots, k$, while

$$\frac{Da_i^R}{Dt} = a_i^R \Big|_j v^j = \dot{a}_i^R - \Lambda_{ji}^\ell a_\ell^R v^j \quad \text{and} \quad \frac{D\pi_i}{Dt} = \pi_i \Big|_j v^j = \dot{\pi}_i - \Lambda_{ji}^\ell \pi_\ell v^j. \quad (25)$$

Equation (24) is the final weak form obtained for the class of constrained mechanical systems examined. This form is convenient for performing an appropriate numerical discretization, leading to improvements in existing numerical schemes based on advanced analytical tools. For the purposes of the present work, this form was first put within the framework of an augmented Lagrangian formulation [16-18]. This leads to a full exploration of the major advantages of the theoretical method applied, in a quite natural manner. More specifically, this method is appropriate for performing a geometrically exact discretization. This is especially useful when the configuration space of the system possesses group properties [19,20]. The success of this formulation was demonstrated by the accurate solution obtained for a number of challenging problems. Some characteristic results are presented next for several typical examples. The first ones have a relatively simple geometry and are of academic interest, while the last example was taken from an industrial application.

Numerical Results

Example 1: Plane Pendulum

The first set of results refers to a planar pendulum, composed of a steel sphere with radius $R = 10 \text{ cm}$, mass $m = 32 \text{ Kg}$ and mass moment of inertia $I_C = \text{diag}(0.13 \ 0.13 \ 0.13) \text{ Kg m}^2$, together with a massless rod with length $L = 1 \text{ m}$. The rod is connected to the ground through a revolute joint so that the system motion is limited in the x-y plane. This system is released from rest, from an initial position, shown in Fig. 1a. Consequently, it undergoes large amplitude oscillations, due to the action of gravity along the negative Y direction.

In Figs 1b-1i are presented and compared numerical results obtained by the new solver (labeled by LMD) with results obtained from a state of the art code, employing a BDF solver [21]. In both cases, an effort was made to keep the same time step and accuracy level in the numerical calculations. In particular, an accuracy level of 0.01 was required in all runs, using either code.

First, in Fig. 1b is shown the mechanical energy of the system as a function of time, assuming a zero potential energy at the position shown in Fig. 1a. Clearly, the commercial code exhibits a gradual and substantial mechanical energy loss. This is probably related to the high level of artificial damping induced in the BDF scheme employed. The consequences of this are demonstrated in Figs 1d-1g. In particular, in Figs 1d and 1e is presented the time history of the vertical component of the displacement at the beginning and at a later time interval of the oscillation. The results indicate a drift and a reduction in the amplitude of oscillation obtained by the BDF method. Similar conclusions are drawn from the results presented in Figs 1f and 1g, presenting the history of the angular velocity of the pendulum. It is important to note that a similar behavior with [21] was also observed by employing another state of the art code in multibody dynamics, which uses also a BDF scheme [22].

The good performance of the new code is due to the fact that the new set of equations of motion employed includes suitable terms, avoiding a growth in the constraint violation error in an automatic manner. For instance, in Fig. 1c is shown the numerical error in the vertical position of the end point of the pendulum. Likewise, in Figs 1h and 1i are shown results obtained by the new code, by taking into account the critical term \bar{m}_{RR} , evaluated by Eq. (19), or neglecting it (i.e., setting it equal to zero) in the calculations. As it is obvious from Eqs (18) and (21), this term assures the presence of the constraint inertia term $\dot{\lambda}^R$ in the equations of motion. Obviously, elimination of this term leads to a sudden and dramatic reduction of the time step, causing a sudden termination of the numerical calculations.

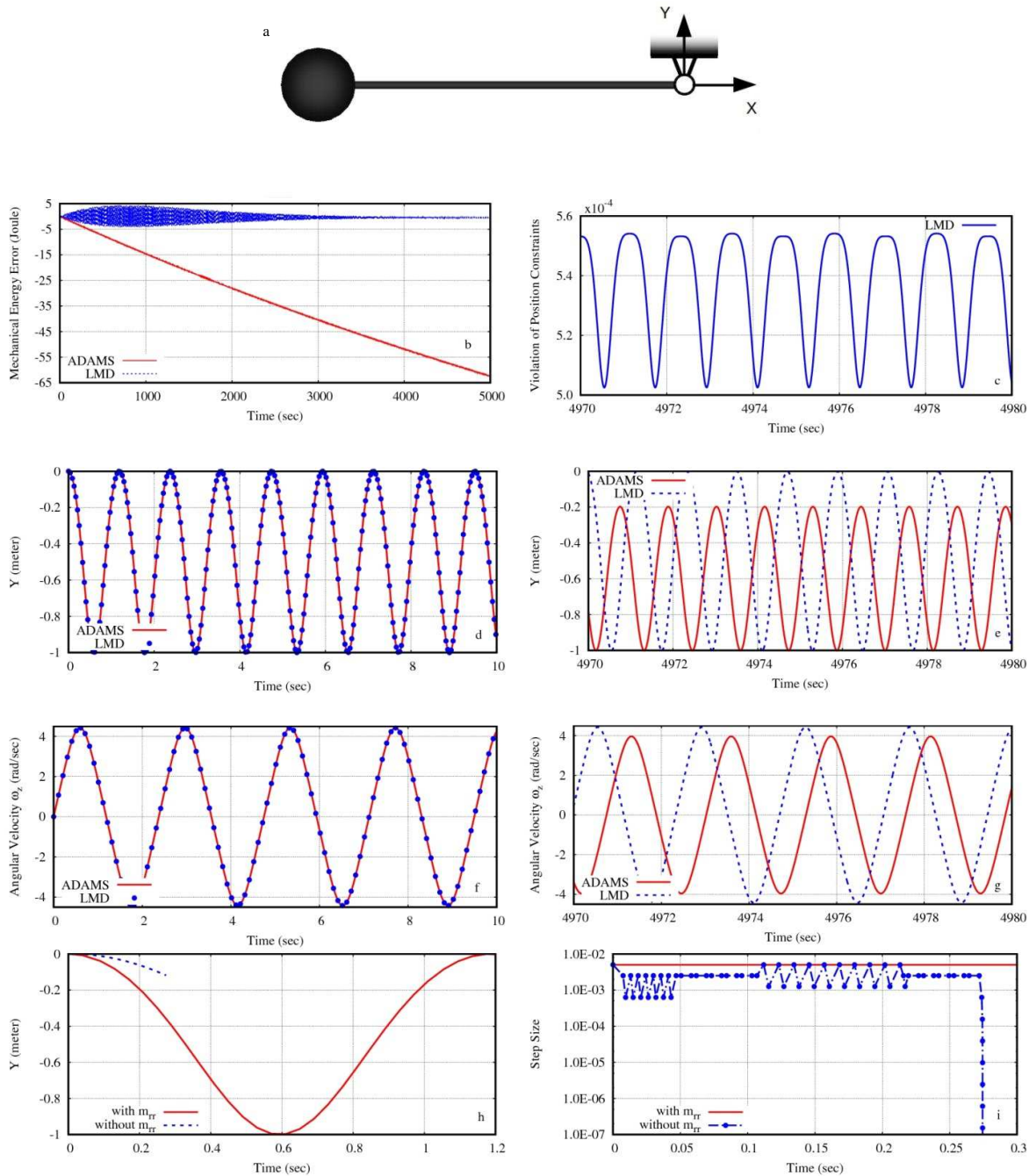


Fig. 1. Numerical results for a planar pendulum: (a) mechanical model, (b) mechanical energy error, (c) violation of position constraint, (d)/(e) history of the sphere Y displacement, (f)/(g) history of the pendulum angular velocity, (h) displacement in the vertical direction Y with and without \bar{m}_{rr} and (i) solver step size with and without \bar{m}_{rr} .

Example 2: Double Four Bar Mechanism

Next, in Fig. 2 are compared results obtained by applying the new method with similar results obtained for a typical benchmark problem [14]. In brief, the double four bar mechanism examined is a representative of a multibody system passing from a singular configuration. All the rods have equal length and uniformly distributed mass. Specifically, when the bars reach the horizontal position, the number of degrees of freedom increases instantaneously from one to three. In the set of calculations presented next, the mechanism starts from rest from the position shown in Fig. 2a and executes oscillations due to the action of gravity along the $-y$ direction. Again, the results of the new method are labeled by LMD.

First, the results of Fig. 2b verify the closeness of the results obtained by the two methods, within the time interval considered. However, the results presented in Fig. 2c demonstrate a difference in the error in the mechanical energy (taking as a reference configuration the one shown in Fig. 2a). The new method predicts a constant value close to zero, which is the exact value. In addition, the results shown in Figs 2d, 2e and 2f show three different types of failure in the response obtained by using the same BDF solver as in the previous example [21]. More specifically, the simulation stops suddenly (Fig. 2d), the solver finds a wrong solution (Fig. 2e) or it predicts a breaking of the connections leading to a disassembling of its members (Fig. 2f), as the mechanism passes from the singular position.

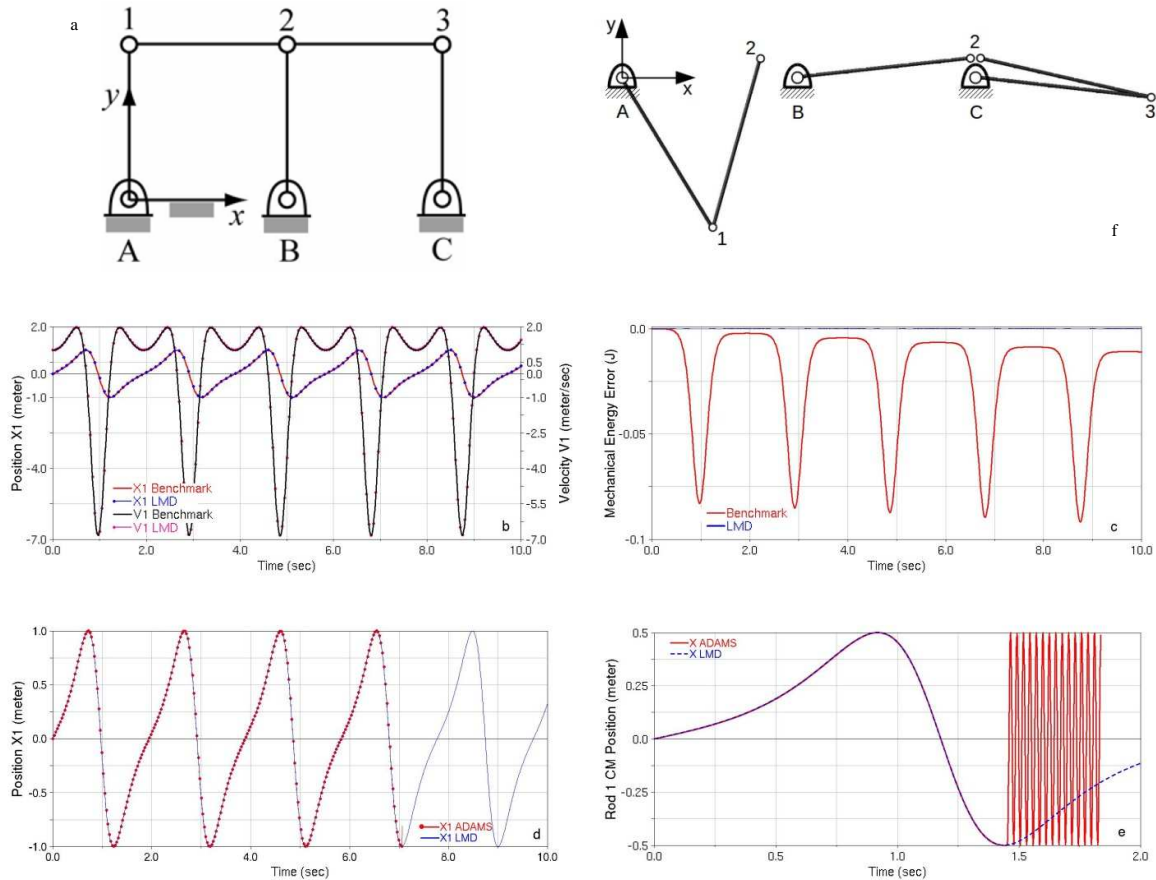


Fig. 2. Numerical results for a double four bar mechanism: (a) mechanical model, (b) history of position and velocity of point P_1 of the mechanism, (c) mechanical energy error, ADAMS results (using a BDF method) where (d) simulation stops, (e) solver finds a wrong solution and (f) the mechanism breaks.

Example 3: Rectangular Bricard Mechanism

The next set of results refers to a six-bar rectangular Bricard mechanism, shown in Fig. 3a. All the rods are connected with revolute joints, have equal length and uniformly distributed mass. Again, this system moves due to gravity acting along the negative y -axis. The mechanism examined represents a mechanical system which is redundantly constrained throughout its motion and, due to this property, it also belongs to a special set of benchmark problems [14].

First, in Fig. 3b are shown the time histories of the x , y and z coordinates of point P_2 , while in Fig. 3c is depicted the mechanical energy of the system. Finally, in Figs 3d and 3e are presented the corresponding histories of the constraint violations in the position and velocity levels during the same time interval, represented by the norm of the array of the constraints at each level.

Direct comparison of the results in Fig. 3 illustrates that the present method is accurate and passes successfully the benchmark tests. It also presents an improved numerical performance. For instance, the mechanical energy computed by the present method remains virtually constant (Fig. 3c). In addition, the errors in both the displacement and velocity constraint violations are bounded and stay at the same level, throughout the time interval examined (Figs 3d and 3e).

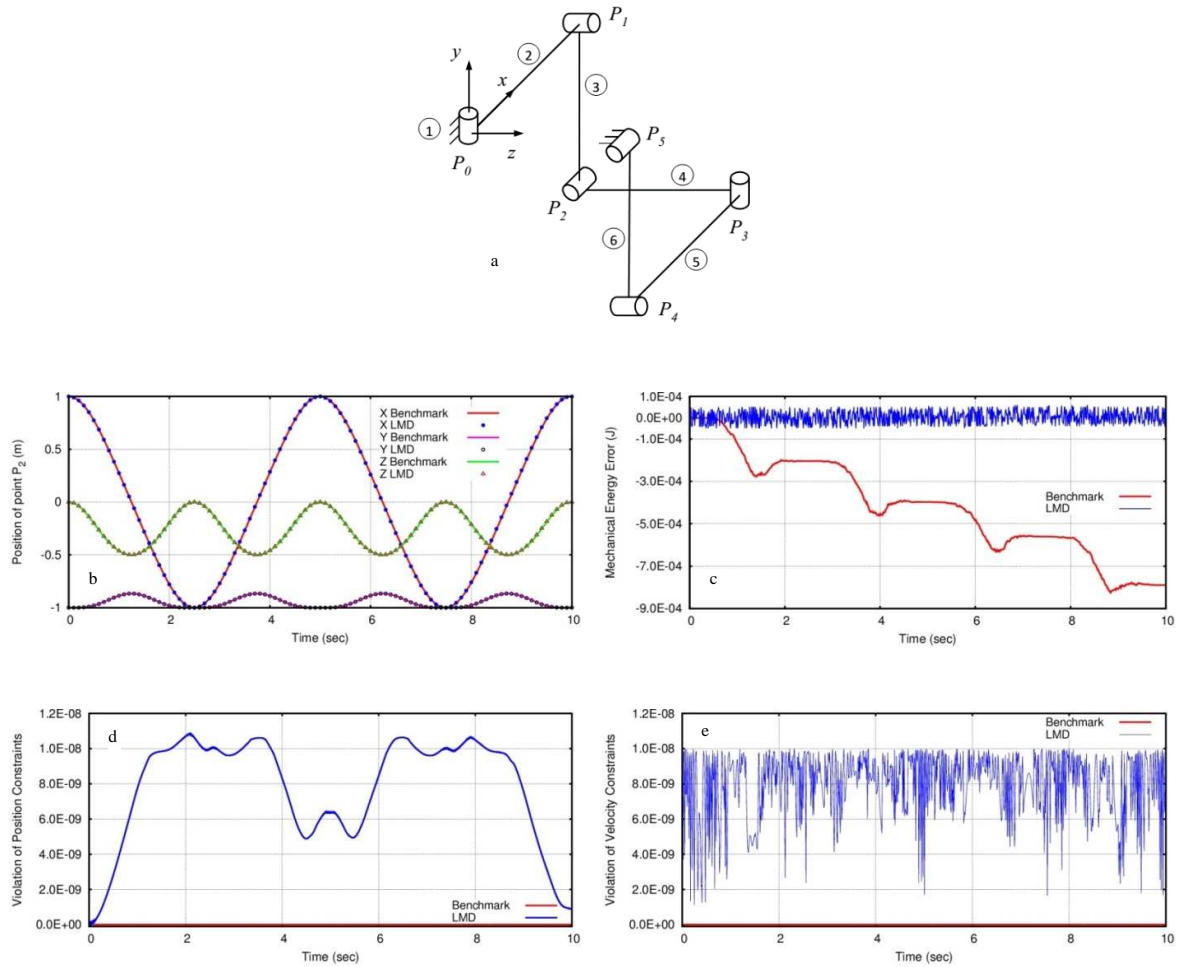
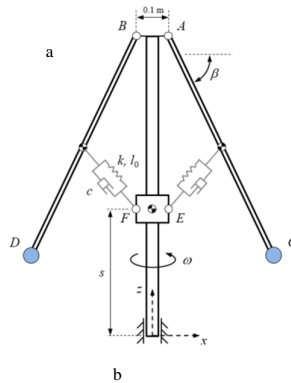


Fig. 3. (a) Mechanical model of a Bricard mechanism, (b) history of the x , y and z coordinates of point P_2 , (c) mechanical energy, (d) violation of position and (e) violation of velocity constraints.

Example 4: Flyball Governor

The next example is a flyball governor, shown in Fig. 4a. Here, the coupler rods have been replaced by spring-damper elements with stiffness and damping coefficients equal to $k = 8 \cdot 10^5$ N/m and $c = 4 \cdot 10^4$ Ns/m, respectively. This produces a stiff system and is included in a special set of benchmark problems [14]. At time $t = 0$, both arms form an angle $\beta = 30^\circ$ with respect to the x -axis and the shaft rotates about its axis with an angular velocity $\omega = 2\pi$ rad/s. Subsequently, the system moves under a gravitational force along the negative z axis.

First, in Figs 2b and 2c are compared results of the new method with a benchmark solution for the history of the angular velocity and the distance s , respectively. The results indicate a good level of agreement. Finally, in Figs 2d and 2e are shown results for the numerical violation observed in the position and velocity constraint, respectively. Clearly, the level of both of these errors is quite low and is controlled by the new methodology developed in an automatic way.



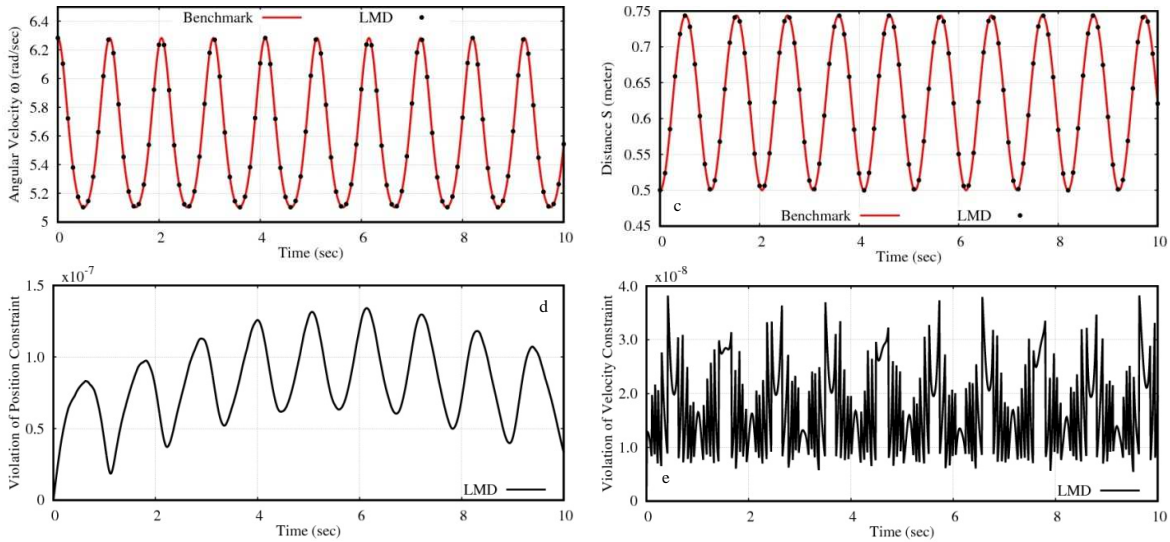


Fig. 4. Numerical results for a flyball governor: (a) mechanical model, (b) history of the angular velocity of shaft, (c) distance S , (d)/(e) violation of constraints in position and velocity field, respectively

Example 5: Rolling Sphere on a Turntable

The system examined next consists of a sphere rolling over a turntable, as shown in Fig. 5a. The special feature of this problem is that it belongs to the class of systems subject to rheonomic constraints. This problem has a long history. For instance, even analytical solutions are available for horizontal and tilted turntables, under pure rolling conditions [23]. Here, a steel ball with a radius of $R = 2,5\text{cm}$ is considered, moving on a horizontal rotating disk. The ball starts at the center of the turntable with a small initial velocity $v_0 = (0.5 \ -0.5 \ 0)^T \text{ m/s}$ and rolls without sliding, while the disk rotates with a constant angular velocity $\Omega_z = 2\pi \text{ rad/s}$ along the vertical axis Z . In Fig. 5b is presented the trajectory obtained for the ball by applying the existing analytical results and the new method developed. As expected by the choice of parameters, the path is circular, while the speed remains constant throughout the whole trajectory.

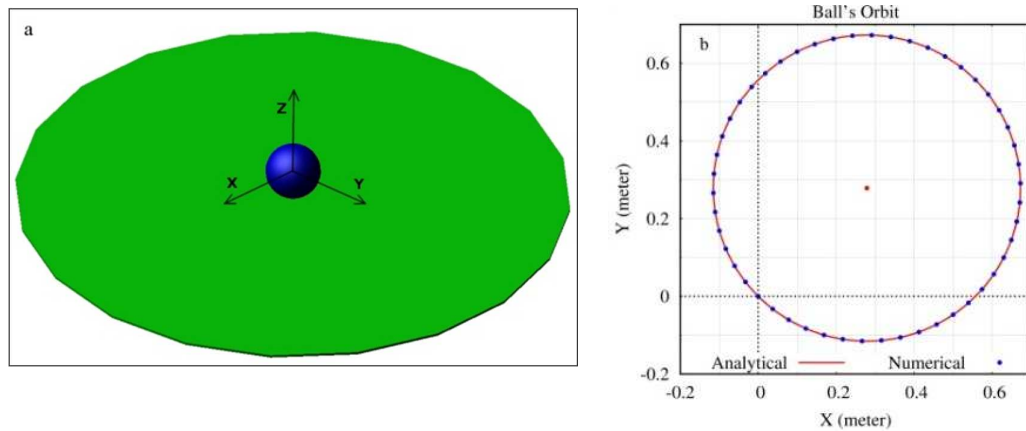


Fig. 5. Numerical results for the rolling ball model: (a) mechanical model and (b) orbit of the ball.

Example 6: Complex Model of a Ground Vehicle

In the last example, a quite complex model of a ground vehicle is examined, shown in Fig. 6a. This model is composed of a basic powertrain system, a complex steering system, together with involved front and rear suspension systems with jounce and rebound bumpers. Also, the tires were modeled using the well-known Pacejka tire model [24]. In total, the model consists of 53 rigid bodies, interconnected with 49 kinematical constraints, 29 bushings, 9 spring-damper systems and 9 action-reaction force elements. As a consequence, the total number of degrees of freedom of the final model is 134. In the examples examined, the vehicle is subjected to two classical road handling tests. For this, an appropriate driving torque and steering angle is applied at the car's differential and wheel during the motion, as shown in Figs 6b

and 6c. In the first test, the vehicle is running over a straight path with a constant longitudinal velocity $V_x \approx -60 \text{ Km/h}$ before it starts performing a typical double lane change (DLC). In Figs 6d and 6f are presented selected results obtained for tire forces and velocity components by applying the new numerical method (labeled by LMD). Moreover, these results are compared with results obtained for the same model by two state of the art numerical codes [21,22]. These codes set up the equations of motion and solve them numerically as a system of DAEs. In the second test, a swept steering maneuver is performed. Typical results for tire forces and velocity components are shown and compared in Figs. 6e and 6g. The difference between the results obtained by the new method and one of the codes [22] is most probably due to differences in the tire models employed.

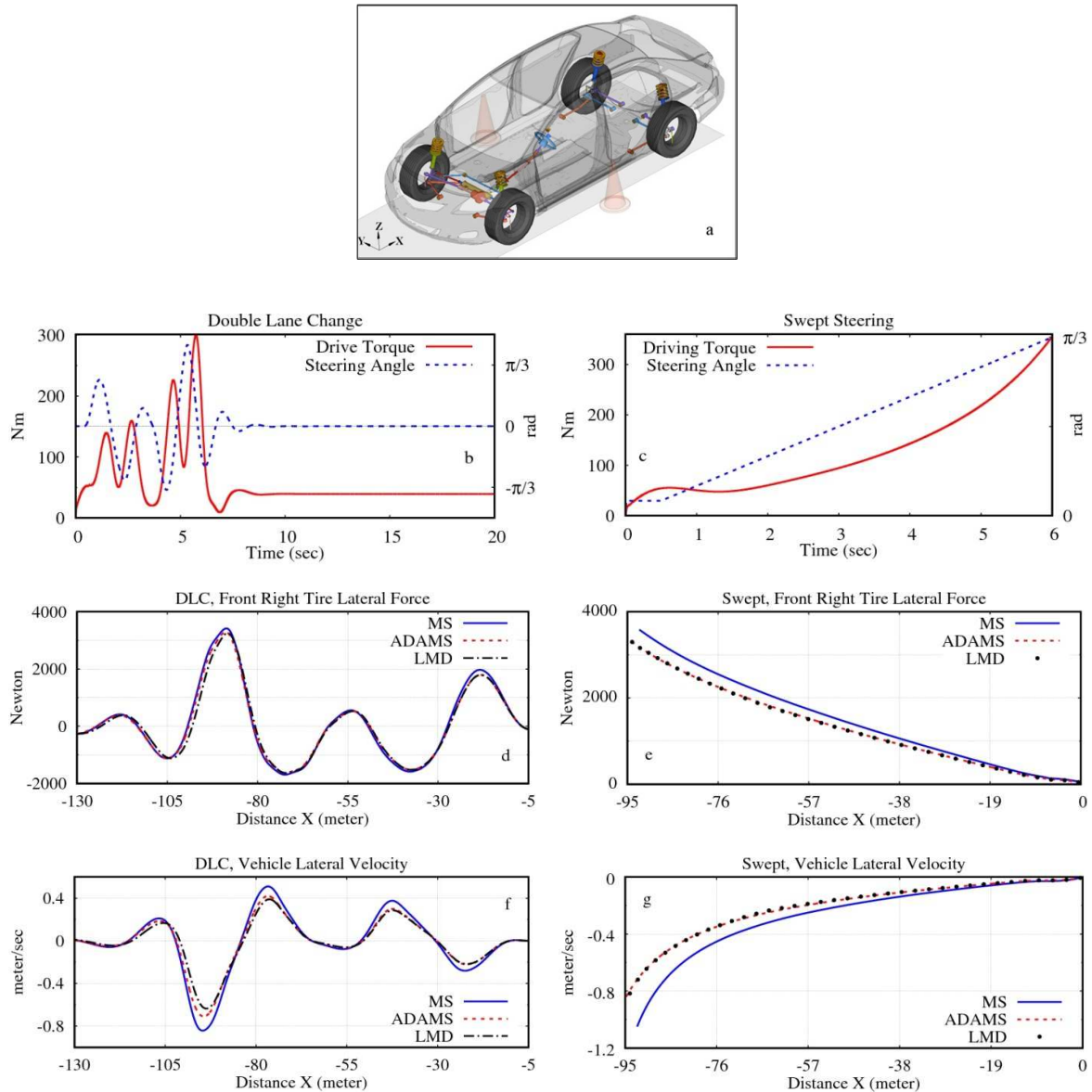


Fig. 6. Numerical results for a car model: (a) vehicle model, (b)/(c) driving torque and steering angle input curves, (d)/(f) front right tire lateral force and vehicle lateral velocity for the DLC analysis, (e)/(g) front right tire lateral force and vehicle lateral velocity for the swept test analysis.

References

- [1] Greenwood, D.T. (1988) Principles of Dynamics. Prentice-Hall Inc., Englewood Cliffs, New Jersey.
- [2] Murray, R.M., Li, Z., Sastry, S.S., A Mathematical Introduction to Robot Manipulation, CRC Press, Boca Raton, Florida, 1994.
- [3] Geraadin, M., Cardona, A., Flexible Multibody Dynamics, John Wiley & Sons, New York, 2001.
- [4] Bloch, A.M. (2003) Nonholonomic Mechanics and Control. Springer-Verlag, New York.
- [5] Shabana, A.A., Dynamics of Multibody Systems, third ed. Cambridge University Press, New York, 2005.

- [6] Bauchau, O.A., Flexible Multibody Dynamics, Springer Science+Business Media, London, 2011.
- [7] Brenan, K.E., Campbell, S.L., Petzhold, L.R., Numerical Solution of Initial-Value Problems in Differential-Algebraic Equations, North-Holland, New York, 1989.
- [8] Marsden, J.E., Ratiu, T.S., Introduction to Mechanics and Symmetry, second ed. Springer Science+ Business Media Inc., New York, 1999.
- [9] Papastavridis, J.G., Tensor Calculus and Analytical Dynamics, CRC Press, Boca Raton, 1999.
- [10] Paraskevopoulos, E., Natsiavas, S., On application of Newton's law to mechanical systems with motion constraints, *Nonlinear Dyn.* 72 (2013) 455-475.
- [11] Natsiavas, S., Paraskevopoulos, E., A set of ordinary differential equations of motion for constrained mechanical systems, *Nonlinear Dyn.* 79 (2015) 1911-1938.
- [12] Rektorys, K., Variational Methods in Mathematics, Science and Engineering, D. Reidel Publishing Company, Dordrecht, 1977.
- [13] Ženišek, A., Nonlinear Elliptic and Evolution Problems and their Finite Element Approximations, Academic Press, London, 1990.
- [14] IFToMM Tech. Comm. for Multibody Dynamics, Library of Computational Benchmark Problems, <http://iftomm-multibody.org/benchmark/>
- [15] Paraskevopoulos, E., Natsiavas, S. (2015) Weak formulation and first order form of the equations of motion for a class of constrained mechanical systems. *Int. J. Non-linear Mech.* 77:208-222.
- [16] Nocedal, J., Wright, S.J., Numerical Optimization, Springer Series in Operations Research, New York, 1999.
- [17] Bayo, E., Ledesma, R., Augmented Lagrangian and mass-orthogonal projection methods for constrained multibody dynamics, *Nonlinear Dyn.* 9 (1996) 113-130.
- [18] Blajer, W., Augmented Lagrangian formulation: geometrical interpretation and application to systems with singularities and redundancy, *Multibody Syst. Dyn.* 8 (2002) 141-159.
- [19] Brüls, O., Cardona, A., Arnold, M., Lie group generalized- α time integration of constrained flexible multibody systems, *Mech. Mach. Theory* 48 (2012) 121-137.
- [20] Paraskevopoulos, E., Natsiavas, S., A new look into the kinematics and dynamics of finite rigid body rotations using Lie group theory, *Int. J. Solids Struct.* 50 (2013) 57-72.
- [21] MSC ADAMS 2016, User Guide, MSC Software Corporation, California, USA.
- [22] MotionSolve v14.0, User Guide, Altair Engineering Inc., Irvine, California, USA.
- [23] Weltner, K., Stable circular orbit of freely moving balls on rotating disks, *Am. J. Phys.* 47 (1979) 984-986.
- [24] Pacejka, H.B., Tyre and Vehicle Dynamics, third ed. Butterworth-Heinemann, 2012.